Advances in Nano Research, *Vol. 9, No. 1 (2020) 1-13*
DOI: https://doi.org/10.12989/anr.2020.9.1.001

Nano-delamination monitoring of BFRP nano-pipes of electrical potential change with ANNs

Wael A. Altabey*[1,2,3], Mohammad Noori [1,4a], Ali Alarjani [3b] and Ying Zhao [1c]

[1] *International Institute for Urban Systems Engineering, Southeast University, Nanjing, Jiangsu, China*
[2] *Department of Mechanical Engineering, Faculty of Engineering, Alexandria University, Alexandria, Egypt*
[3] *Department of Mechanical Engineering, College of Engineering in Alkharj, Prince Sattam Bin Abdelaziz University, Alkharj 11942, Saudi Arabia*
[4] *Department of Mechanical Engineering, California Polytechnic State University, San Luis Obispo, CA, USA*

(*Received July 9, 2018, Revised October 8, 2019, Accepted December 24, 2019*)

Abstract. In this work, the electrical potential (EP) technique with an artificial neural networks (*ANNs*) for monitoring of nanostructures are used for the first time. This study employs an expert system to identify size and localize hidden nano-delamination (*N.Del*) inside layers of nano-pipe (*N.P*) manufactured from Basalt Fiber Reinforced Polymer (BFRP) laminate composite by using low-cost monitoring method of electrical potential (EP) technique with an artificial neural networks (*ANNs*), which are combined to decrease detection effort to discern *N.Del* location/size inside the *N.P* layers, with high accuracy, simple and low-cost. The dielectric properties of the *N.P* material are measured before and after *N.Del* introduced using arrays of electrical contacts and the variation in capacitance values, capacitance change and node potential distribution are analyzed. Using these changes in electrical potential due to *N.Del*, a finite element (FE) simulation model for *N.Del* location/size detection is generated by ANSYS and MATLAB, which are combined to simulate sensor characteristic, therefore, FE analyses are employed to make sets of data for the learning of the *ANNs*. The method is applied for the *N.Del* monitoring, to minimize the number of FE analysis in order to keep the cost and save the time of the assessment to a minimum. The FE results are in excellent agreement with an ANN and the experimental results available in the literature, thus validating the accuracy and reliability of the proposed technique.

Keywords: nano pipes; nano-delamination monitoring; Electrical Capacitance Sensor (ECS); BFRP; FEM; ANNs

1. Introduction

Nano pipes (*N.Ps*) manufactured from laminate composite materials are widely used in many nanoelectro-mechanical systems. Thus understanding the mechanical behavior of these nanostructures is much needed for design and development of a new class of nano-systems such as nano-actuators and nano-sensors. But the effect of internal defects may significantly change the stiffness and reduce the strength and lifetime of these composite nanostructures (Altabey 2017a, b).

Delamination is one of the most common damages that can occur between layers in layered composite materials. In general, it can be caused due to manufacturing faults or service process effects such as impact loads, fatigue, etc. Better understanding of delamination mechanism in laminated composite materials will allow to increase use this material in nonstructural applications. The delamination detection in general is a very difficult and expensive job in particular *N.Del* in *N.Ps* from laminated composites becomes near impossible. This difficulty of detection indicate to the importance of development of easy and economical technique for monitoring *N.Del* in that type of *N.Ps* (Zhao *et al*. 2017a, 2018a, b, 2019a, Altabey and Noori 2018a, Kost *et al*. 2019).

Several methods have been found to be useful for in-situ evaluation of composite nanostructures, where the structural integrity of that nanostructures manufactured from laminate composite can be assessed effectively. Recently, various methods have been implemented for that nanostructures monitoring include Ultrasonic; X-Ray Radiography and Thermography (Zhao *et al*. 2017b, 2018c, 2019b, Noori *et al*. 2018, Ghiasi *et al*. 2019).

Although, there is a diverse range of techniques for assessment composite nanostructures, the researchers were found the capabilities and limitations of each method are different, where each technique has its specific field of applicability although there is a level of overlap based on the type and accuracy of detection and the ability to detect more data of damage identification. For instance, it may be necessary to combine information obtained from acoustic emission and X-ray radiography to achieve a three-dimensional map of the complex array of delamination location/size in a composite, however, no single method is capable of easily detecting, or identifying delamination with high level of accuracy, and at a low-cost (Mouritz 2003, Altabey 2017c, d, 2018, Al-Tabey 2014).

ECS is one of the most mature and promising of new

*Corresponding author, Associate Professor,
E-mail: wael.altabey@gmail.com
[a] Professor, E-mail: mnoori@outlook.com
[b] Student
[c] Professor

http://www.techno-press.org/?journal=journal=anr&subpage=5
ISSN: 2287-237X (Print), 2287-2388 (Online)

methods, which measures the capacitance change of multi-electrode/nanoelectrode sensor due to the change in dielectric permittivity. It has the characteristics such as being a low cost, fast response, non-intrusive method with a broad range of applications and with a high level of safety (Yang *et al.* 1995a, b, Li and Huang 2000, Mohamad *et al.* 2012, Zhang *et al.* 2014).

As a result in our previous works by Altabey (2017e, f) and Altabey *et al.* (2018), the present method had been successfully assessment of the delamination location/size, crack identification (Altabey and Noori 2017), water absorption level (Altabey and Noori 2018b) in composite pipes and tensile creep monitoring of composite plates (Altabey *et al*. 2019). But they found a lot of FE calculations must be performed to obtain a sufficient number of sets of electric potential differences. This is the main drawback of the method identified so far.

In this study, we applied the previous electrical potential (EP) technique in *N.Ps* manufactured from BFRP laminate composite materials to improve one of most common nanostructures (e.g., nano-diaphragms, nano-pipes), which used in nanoelectro-mechanical systems. In order to avoid main drawback of this method, a FEM is generated with an artificial neural networks (*ANNs*), which are combined to decrease detection effort to discern *N.Del* location/size inside the *N.P* layers, with high accuracy, simple and low-cost. By ANSYS and MATLAB, split into four scenarios only of *N.Del* location/size and learning of the *ANNs* under each *N.Del* scenario. The *ANNs* are adopted as solvers to obtain relationships between the electric potential differences and the *N.Del* location/size in order to keep the cost and save the time of the FE assessment data to a minimum. Our presented technique results are showed the excellent agreement between FE and ANN results.

2. Principle of Electrical Capacitance Sensor (ECS)

ECS was first introduced in the 1980s by a group of researchers from the US Department of Energy, at Morgantown Energy Technology Center (*METC*), to measure fluidized bed systems (Fasching and Smith 1988, 1991, Huang *et al*. 1989). The technique further developed and advanced rapidly during the past 10 years. It has gained attention and found important applications in monitoring industrial processes, due to its low cost and its operability under harsh environmental conditions.

ECS converts the permittivity of the piping system to inter-electrode capacitance, which is the *ECS* forward problem. Capacitance measuring circuit takes the capacitance data and transfers that to imaging computer. Imaging computer reconstructs the distribution image with a suitable algorithm, which is called *ECS* inverse problem.

The need for a more accurate measurement of *ECS* has led to the study of the factors which influence and affect *ECS* sensitivity and the sensitive domain of *ECS* electrodes. In general, there are three factors that have been studied and found that they affect *ECS* measurements, e.g., Monitoring target manufacturing material (Jaworski and Bolton 2000, Pei and Wang 2009, Al-Tabey 2010, Asencio *et al*. 2015, Sardeshpande *et al*. 2015, Mohamad *et al*. 2016, Altabey 2016a) and Monitoring target thickness (Daoye *et al*. 2009, Altabey 2016b). Altabey (2016c) found that the environmental temperature also affect *ECS* sensitivity and sensitive domain of *ECS* electrodes with high percentage. Therefore, it was concluded that the environmental temperature should be considered as the fourth factor which influences the *ECS* measurement sensitivity.

Fig. 1 is a schematic representation of an expert system for *N.Del* assessment using electrical potential (EP) technique with an *ANNs*, in which R_1 is inner *N.P* radius; R_2 is outer *N.P* radius; R_3 is earthed screen radius. The *ECS* also includes radial guard electrodes to constrain the field lines from the excited nano-electrode (*N.E*) and to reduce the dependence of spacing between the nano-electrodes (*N.Es*) and the screen as shown in the Fig. 1. The function of the sensor includes measuring the capacitance between all possible combination pairs of the *N.Es* and converting the measured capacitance values in the voltage signals. The sensors physical specifications and the permittivity values of BFRP *N.Ps* are shown in Table 1.

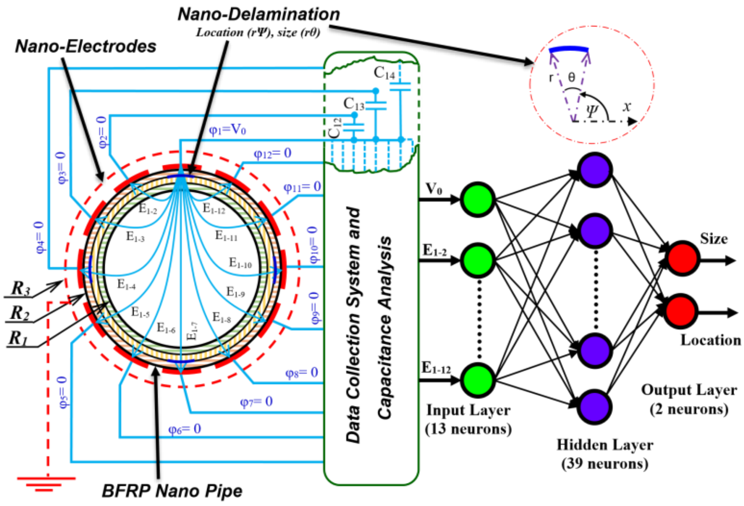

Fig. 1 Schematic representation of the *N.Del* monitoring method using an *ECS* method with an *ANNs*

Table 1 Sensor physical specification

***ECS* system**	**Specification**
No. of Nano-electrodes	12
Space Nano-electrodes	2 nm
Nano Pipe diameter (d_i)	94 nm
Nano Pipe thickness (h)	6 nm
Earth Screen diameter	110 nm
Thickness of Nano-electrodes	1 nm
height of Nano-electrodes	0.3 μm
Permittivity Basalt fiber/Polymer	ε_b = 2.2 Fm^{-1}
Permittivity of Water	ε_w = 80 Fm^{-1}
Permittivity of Air	ε_a = 1.0 Fm^{-1}
Excitation voltage	φ = 15 mV

*Remark: Other parameters of the electrical property can be found in Zhao *et al*. (2018a)

The electric potential differences of each segment between *N.Es* are measured for various scenarios of *N.Del* location/size. From the measured data, the relationships between electric potential differences and *N.Del* location/size are obtained using an *ANNs*.

3. Finite element simulation model

3.1 Physical properties of the BFRP N.P

Table 2 list all the parameters required for physical and mechanical properties of the BFRP laminate composite. These FRP composite properties were tested at the National and Local Joint Engineering Research Center for FRP Production and Application Technology, Nanjing, China, a high-tech company specialized in the research and development, manufacturing, marketing and technical assessment of high-performance fibers and composites. To examine the effect of *N.Del* on the dielectric properties in BFRP laminated panel, the FE analysis of the electric field intensity of laminated panel were designed using ANSYS ver.15. Suitable finite elements were selected and employed to simulate FRP properties, i.e., PLANE121 element is used to simulate nano-structural property, triangular 6-node, and the element has one degree of freedom, voltage, at each node, and SOLID123 is used to simulate electrical property.

3.2 ECS governing equations

In terms of Electrical Capacitance sensor (ECS), the forward problem is the problem of calculating the capacitance matrix C from a given set of sensor design parameters and a given cross-sectional permittivity distribution $\varepsilon(x, y)$. Thus, the system was governed by the following Poisson equation

$$\nabla . \varepsilon(x, y)\nabla\varphi(x, y) = 0 \tag{1}$$

Where: $\varphi(x, y)$ is the potential distribution inside the *ECS* was determined by solving the Poisson's equation. For tlatktj the boundary condition imposed on the *ECS* head by the measurement system. The electric field vector $E(x, y)$, the electric flux density $D(x, y)$ and the potential function $\varphi(x, y)$ are related as follows

$$E(x, y) = -\nabla\varphi(x, y) \tag{2}$$

$$D = \varepsilon(x, y)E(x, y) \tag{3}$$

The change on the *N.Es*, and hence the inter *N.E* capacitances could be found using the definition of the capacitance and Gauss's law based on the following surface integral

$$Q_{ij} = \oint_{S_j} (\varepsilon(x, y)\nabla\varphi(x, y). \hat{n})\, ds \tag{4}$$

where: $\nabla . \varepsilon(x, y)$ is the divergence of permittivity distribution, $\nabla\varphi(x, y)$ is the gradient of potential distribution, S_j is a surface enclosing electrode j, ds is an infinitesimal area on electrode j, $\hat{n}$ is the unit vector normal to S_j and ds is an infinitesimal area on that.

3.3 The boundary conditions

The potential boundary conditions were applied to the sensor-plate (nano-electrodes). For one *N.E*, the boundary condition of electric potential ($V = V_0$) with 15 mV (V_0) was applied and another *N.Es* was kept at ground ($V = 0$) potential to simulate a 15 mV (RMS) potential gradient across the *N.Es*. For representing the natural propagation of electric field, the default boundary condition of continuity ($\hat{n}.(D1 - D2) = 0$) was maintained for the internal boundaries.

4. Artificial Neural Network (ANN) Modeling

The *RBNN* has three layers consisting of an input, a unique hidden layer (function) and an output layer. The input layer is composed of input data and the output layer produces the network response. The function layer is an intermediate layer between the input and the output layer. The activation function of the neurons of the hidden layer is a Gaussian transfer function

Table 2 Physical and mechanical properties of the BFRP

EX	***EY = EZ***	***GXY = GXZ***	***GYZ***	***PRXY = PRXZ***	***PRYZ***	***rho***
96.74 GPa	22.55 GPa	10.64 GPa	8.73 GPa	0.3	0.6	2700 kg/m^3

*Remark: rho is material density, EX, EY, EZ are elastic modulus in the X, Y and Z directions respectively, GXY, GYZ, GXZ are Shear modulus in the XY, YZ and XZ Planes respectively, PRXY, PRYZ, PRXZ are Poisson's Coefficient in the XY, YZ and XZ Planes respectively

$$\Phi(x) = exp\left[-\left(\sum_{j=1}^{jj}\left\|x_j - c_i\right\|^2 \Big/ 2\sigma_i^2\right)\right] \quad (5)$$

where (x) is the input vector, c_i is the center of a region called a receptive field, σ_i is the width of the receptive field, $\Phi(x)$ is the output of the i^{th} neuron, and i is the number of neurons.

RBNN Network can learn faster than Feed-Forward Neural Networks (*FFNN*) and requires less training data. The performance of the *RBNN* essentially depends on the chosen center where the value of the function is higher and the spread, which indicates the radial distance from the radial basis function (RBF) center, in which the function value resides, is significantly different from zero (Buhmann 2003). The spread value in this work is selected arbitrarily based on the minimum error criteria.

4.2 Performance evaluation measures

It is very useful from the designer's point of view to have a neural system that helps decide whether its suggested design is appropriate or not by calculating the Mean Square error (MSE) from the equation

$$MSE = \sum\left(\left(E_{ij}\right)_{nn} - E_{ij}\right)^2 / n \quad (6)$$

where $\left(E_{ij}\right)_{nn}$ the predicted electric potential differences, E_{ij} the electric potential differences measured from FE method, and n is the number of FE measured data values.

Thus, the performance index will have either an overall minimum, depending on the characteristics of the input vectors. The local minimum is the minimum of a function over a limited range of input values. The local minimum is unavoidable when the ANN is installed. Thus, a local minimum may be good or bad depending on the proximity of the local minimum to the global minimum and how much an MSE is required. In any case, the method applied to solve this problem and go down the local minimum with momentum. Momentum allows a network to respond not only to the local gradient, but also to recent trends in the error surface. Without dynamism, a network can become stuck in a shallow local minimum.

The estimation performances of *N.Del* location/size is evaluated by the lack of fit with the adjusted coefficient of the multiple determination $R^2{}_{adj}$ (Myers and Montgomery 2002, Jiang *et al.* 2014); $R^2{}_{adj}$ is defined as

$$R^2{}_{adj} = 1 - \frac{SS_E/(n-k-1)}{S_{yy}/(n-1)} \quad (7)$$

The value of $R^2{}_{adj}$ is equal to or less than 1.0. A higher value of $R^2{}_{adj}$ implies a better fit. When the ANN shows a very good fit, $R^2{}_{adj}$ approaches 1.0. A good fit of the ANN means that the ANN gives good gives good estimates for the change in dielectric properties used for the regression. Lower $R^2{}_{adj}$ values mean lower estimations and the error band of the estimated result is wider.

5. Results and discussion

5.1 Convergence study and accuracy

In this subsection, a convergence study is carried out for the proposed method, the differences of electrical potential of normalization between the electrodes due to the delamination are calculated and compared with the experimental results available in the literatures. The dataset used for the validation of the presented technique is adapted from Todoroki *et al.* (2004). The tests were carried out on laminated composite beams made from unidirectional carbon/epoxy (CFRE) layers, the stacking sequence is $[0_2/90_2]_s$ and the thickness of the laminates is approximately $t = 1$ *mm*. The volume fraction of fiber is approximately $V_f = 0.5$. The beam type specimens have a length of *270 mm* and a width of *15 mm*. Seven electrodes are mounted on the surface of the sample. All of these electrodes are placed on one side of a sample. For the electrode model, the thickness of the electrodes is *10 mm*, the space between the electrodes is *45 mm* and the limit condition of the electric potential (V = V_0) with + 5V (V_0). The electrical potential changes of each segment between the electrodes are measured for various cases of location and size of delamination. From the measured data, the relationships between the electrical potential change and the location and size of the delaminations are obtained using the surface response method. Table 3 presents a convergence and comparison study for the proposed method data and the experimental data of Todoroki *et al.* (2004).

Table 3 presented a comparison between finite element (FE) data and experimental results available in the literature, it can be seen that the numerical results are in excellent agreement with the experimental results of the electric potential differences of normalization presented by Todoroki *et al*. (2004). This validates the precision of the technique presented.

5.2 Electrical Potential (EP) technique for Nano-Delamination (N.Del) monitoring

To study the effect of *N.Del* on the dielectric properties of *N.P* material, FE analysis of the electric field intensity of the BFRP piping system was performed using commercially available 2D ANSYS software, ANSYS (The Electrostatic Module in the Electromagnetic subsection of ANSYS 2015, Al-Tabey 2012, Altabey *et al.* 2018a, b). The software calculates only the potential and electric field values at the element nodes and interpolates between these nodes to obtain the values of other points in the elements.

The simulations and the potential distribution of the nodes of the *N.P* before and after the *N.Del* initiated for the ANSYS 2D simulation, when the *N.E* (1) is excited, are illustrated in Fig. 2 respectively to the right and to the left.

The blue area represents the region of the potential-free *N.P* i.e., $\varphi = 0$ but the colored areas represent the region of the *N.P* having the different potential (different node potential), the area of the electrode can be sensitive or domain detection.

Table 3 Convergence study of normalization electrical potential differences of the CFRE laminated composite beams

$e_{1\text{-}2}$	(1)	0.9918	0.2922	0.6931	0	0	0.6315	0.1897	0.0105	0.3158	0.0184
	(2)	0.9914	0.2873	0.6877	0	-0.0057	0.6007	0.1869	0.0059	0.3111	0.0139
$e_{2\text{-}3}$	(1)	0.0015	0.3512	0.7177	0.1683	0	0.3724	0.3711	0.0158	0.4531	0.0187
	(2)	-0.1305	0.3478	0.7127	0.1669	-0.0172	0.3682	0.3686	0.0094	0.4470	0.0139
$e_{3\text{-}4}$	(1)	0	0.4497	0.1380	0.5911	0.5125	0.5848	0.7355	0.0008	0.3992	0
	(2)	0	0.4461	0.1375	0.5881	0.5113	0.5813	0.7294	0	0.3976	0
$e_{4\text{-}5}$	(1)	0	0.5243	0.0173	0.6786	0.7826	0.4106	0.5473	0	0.5481	0.2392
	(2)	0	0.5217	0.0125	0.6754	0.7814	0.4069	0.5451	0	0.5457	0.2371
$e_{5\text{-}6}$	(1)	0	0.3269	0	0.3721	0.2894	0.0006	0	0.5900	0.4711	0.2671
	(2)	0	0.3251	-0.0125	0.3698	0.2873	0	0	0.5885	0.4692	0.2650
$e_{6\text{-}7}$	(1)	0	0.4699	0	0.1856	0.2175	0	0	0.8111	0.1683	0.9369
	(2)	0	0.4687	0	0.1823	0.2126	0.0065	-0.0026	0.8085	0.1655	0.9344
Location	(1)	-127.35	-113.23	-81.53	-68.37	-18.22	7.86	19.58	67.34	97.39	108.19
	(2)	-127.5	-113.5	-82	-69	-18.5	8	20	68	98	109
Size	(1)	5.48	4.87	1.96	5.46	5.92	2.91	5.96	8.48	5.98	4.95
	(2)	5.5	5	2	5.5	6	3	6	8.5	6	5

(1) Proposed method, (2) Todoroki *et al*. (2004)

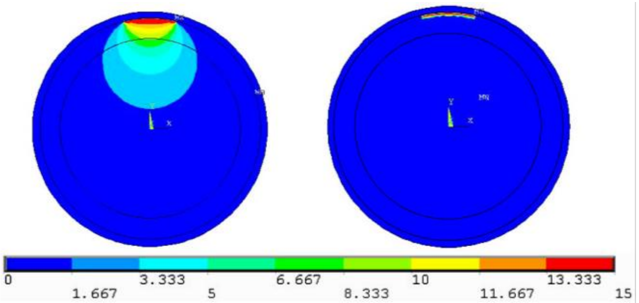

Fig. 2 The node potential distribution of BFRP *N.P* before embedded *N.Del* right and after embedded *N.Del* left

From the FE simulation shown in Fig. 2, we can conclude that this is a significant difference before and after the *N.Del* introduced into the potential of the node and the intensity of the electric field.

The capacitance values between the *N.Es* (C_{ij}) and the potential differences (E_{ij}) of the 2D simulations are calculated before the $N.Del_0$ and after $N.Del_i$, where $i = 1, 2$ .... is the number of scenarios of *N.Del* (FE models). In general, this study must use at least 66 different FE model of *N.Del* scenarios ($N.Del_i$) (Eq. (8)) to validate the accuracy and reliability of the proposed technique, which means a great effort and a high cost, also very long time to assess *N.Del* location/size.

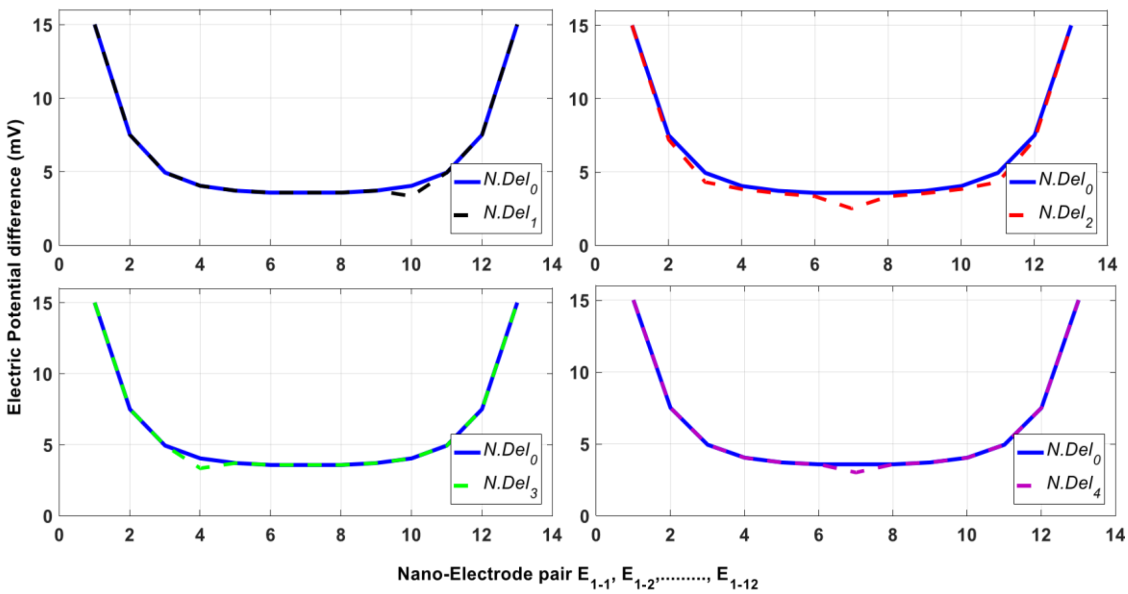

Fig. 3 Effect of $N.Del_i$ on electric potential difference (mV) when *N.E* (1) is excited

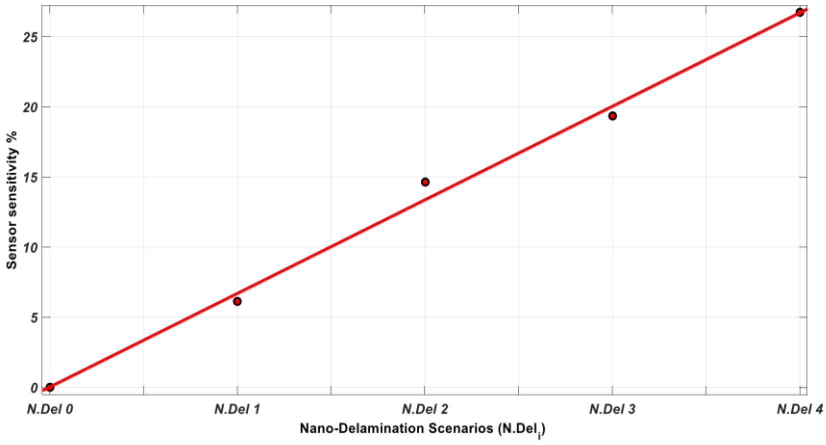

Fig. 4 *ECS* sensitivity versus *N.Del$_i$*

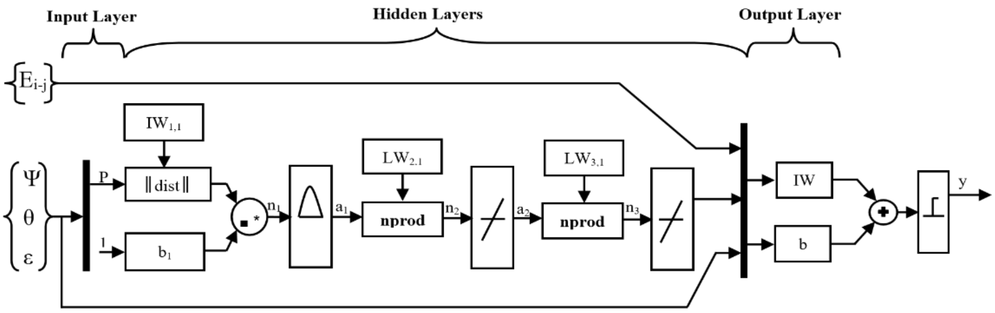

Fig. 5 Schematic illustration of *RBNN* design for present study with input data Ψ, θ, ε

$$M = \frac{N(N-1)}{2} \tag{8}$$

where N is the number of *N.Es*, and M is the number of *N.Del* scenarios.

In this study, an electrical potential (EP) technique is applied with artificial neural networks (*ANNs*), which are combined to decrease the detection effort to discern the location / size of the *N.Del* by minimizing the number of FE models in order to keep save the time of the *N.Del* assessment to a minimum. The method has successfully monitored the *N.Del* location / size using only four scenarios instead of 66 scenarios, the first scenario (*N.Del$_1$*) has a size $\theta = 5^o$, is located at $r = 51\ nm$ and $\Psi = 0^o$, the second scenario (*N.Del$_2$*) has the size $\theta = 10^o$, is located at $r = 51\ nm$ and $\Psi = 90^o$, the third scenario (*N.Del$_3$*) has the size $\theta = 15^o$, is located at $r = 51\ nm$ and $\Psi = 180^o$ and the final scenario (*N.Del$_4$*) has the size $\theta = 20^o$, is located at $r = 51\ nm$ and $\Psi = 270^o$, respectively, as shown in Table 4.

As shown in Fig. 3 and Table 4 of the node potential differences (E_{i-j}) with different *N.Del* scenarios when the electrode (1) is excited, we can be seen that the effect of *N.Del* has occurred on the potential of node distributions the degradation in the potential differences occurred, this degradation is according to the *N.E* that mounted near the *N.Del* location occurred (for example the degradation in the value E_{1-4} is due in the *N.Del* scenario (*N.Del$_3$*), value E_{1-7} is due to the scenario (*N.Del$_4$*) and the value E_{1-10} is due to the scenario (*N.Del$_1$*)), except that the scenario (*N.Del$_2$*) is influenced by all the values potential differences from E_{1-2} to E_{1-12} because the *N.Del* is located near the *N.E* (1), and so this behavior will be repeated when the other *N.Es* are excite (see Fig. 1).

Fig. 4 shows the *ECS* sensitivity versus *N.Del* scenarios (*N.Del$_i$*). The *ECS* sensitivity is defined as

$$ECS\ sensitivity\% = \frac{C_{del_0} - C_{del_i}}{C_{del_0}} \times 100 \tag{9}$$

where: C_{del0} and C_{del} are the capacitance measurements for before and after *N.Del* started respectively.

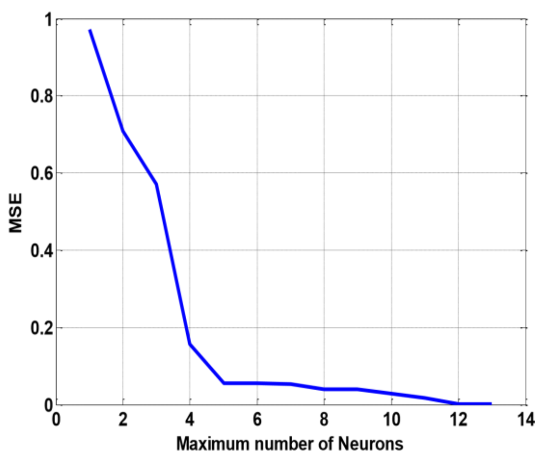

Fig. 6 The relation between Mean Square error (MSE) and the number of hidden layer neurons

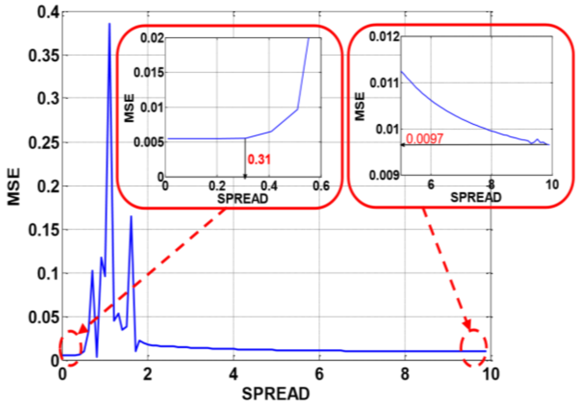

Fig. 7 The relation between Mean Square error (MSE) and selected spread parameters

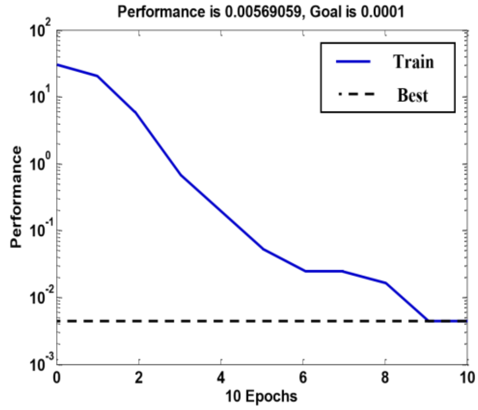

Fig. 8 Training performance of suggested RBNN

As shown in Fig. 4, the sensitivity of the *ECS* depends on the *N.Del* size (θ), the *ECS* sensitivity increase with *N.Del* size increases, the sensitivity of the sensor varies between 6.13 and 26.723% for the scenario ($N.Del_1$) to scenario ($N.Del_4$) respectively and the selected *ECS* geometry parameters.

5.3 RBNN structure design and learning

A *RBNN* structure is designed based on one input layer, three hidden layers and one output layer respectively as shown in Fig. 1. The first hidden layer with radial basis neurons while the second and third layer with pure linear ones as shown in Fig. 5.

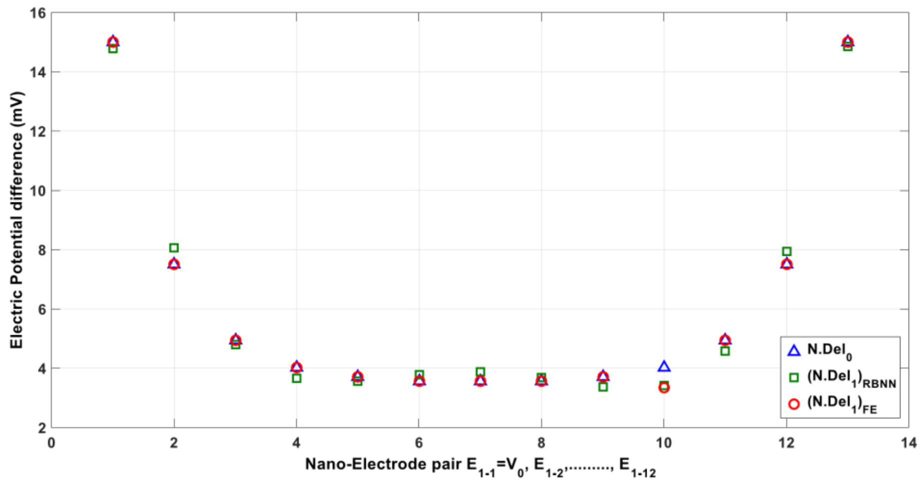

(a) Predicted data

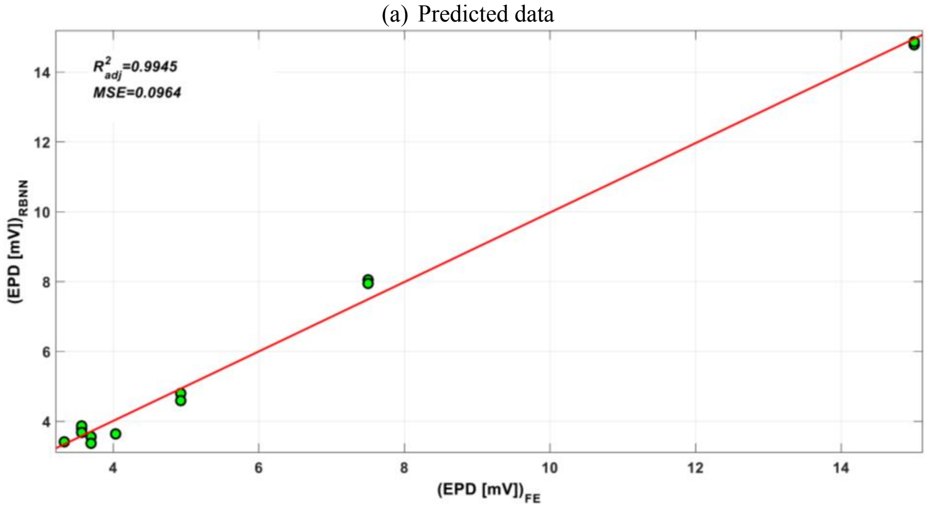

(b) Performance

Fig. 9 Comparison between the Finite Element (FE) data and Radial Basis neural networks (RBNN) predicted data for nano-delamination scenario ($N.Del_1$)

Learning vectors formed the initial centers of Gaussian RBFs. Determination of the hidden layer, in addition to the number of nodes in the input and output layers, to provide the best training results, was the initial phase of the training procedure. The goal of MSE to reach at the end of the simulations was 0.0001. Since the second step was largely a trial-and-error process, and involved *RBNNs* with the number of hidden layer neurons more than 13, it did not show any sizeable improvement in prediction accuracy. Thus the number of neurons (the number of RBFs) for the single hidden layer was selected as 13 neurons. Selection of the number of hidden layer neurons, with respect to the MSE term in the presence of different spread parameterized *RBNNs* is shown in Fig. 6.

Choosing an appropriate spread constant will increase the accuracy of the network. The spread (the width of the RBFs') constant of radial basis function was selected by using Genetic Algorithm (GA). GA may have the tendency to converge towards local optimum (Valle *et al*. 2008) rather than the global optimum of the problem, if the fitness function is not defined properly. The optimum spread parameter was selected as constant for all group of permittivity, after the trials with the selected hidden layer neurons number, the spread constant was selected as 0.31 as shown in Fig. 7.

5.4 Nano-Delamination (N.Del) location/size estimation using Radial Basis Neural Networks (RBNN)

RBNN is trained by measuring values of Ψ, θ, ε to predict the potential differences (EPD) $E_{i\text{-}j}$. In the first *RBNN* structure is applied for training the data of *ECS* in Table 4. Fig. 8 shows the training performance of suggested *RBNN*.

Figs. 9 and 10 represent the comparison between the FE data and the *RBNN* predicted data for *N.Del* scenarios ($N.Del_1$) and ($N.Del_3$). The results of the *RBNN* show much satisfactory predication quality for this case study. The value of mean square error (MSE) between the FE and *RBNN* predicted data for scenarios ($N.Del_1$) and ($N.Del_3$), in order to obtain the best performances of the present neural network are 0.0964 and 0.044 respectively. The adjusted coefficient R^2_{adj} of the predicted result is 0.9945 and 0.9985 for scenarios ($N.Del_1$) and ($N.Del_3$) respectively.

Figs. 11 and 12 show the comparison between the FE

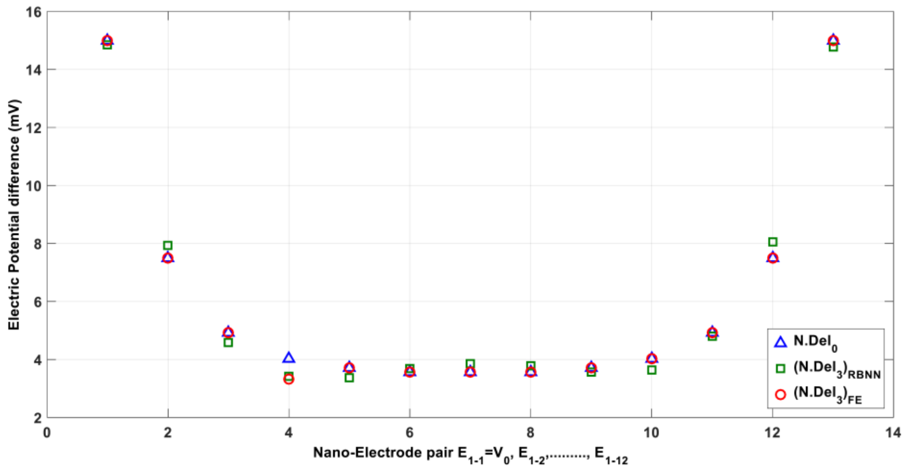

(a) Predicted data

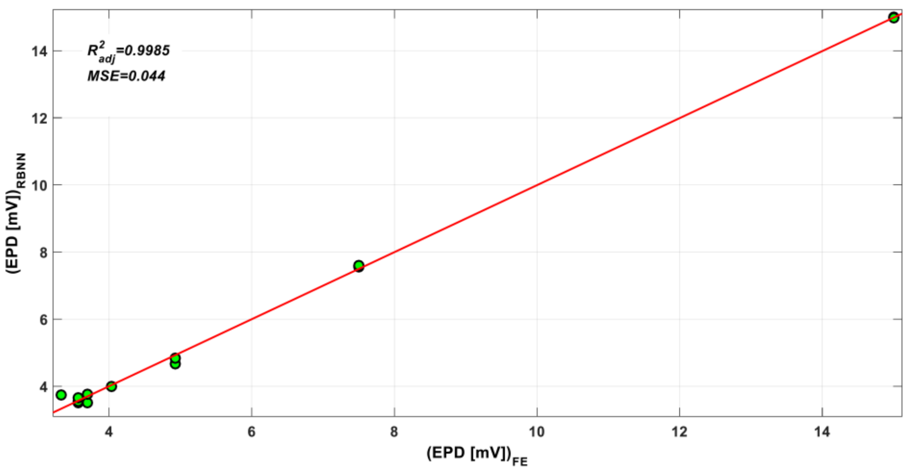

(b) Performance

Fig. 10 Comparison between the Finite Element (FE) data and Radial Basis neural networks (RBNN) predicted data for nano-delamination scenario ($N.Del_3$)

data and the Radial Basis neural networks (*RBNN*) expected data for *N.Del* scenarios ($N.Del_2$) and ($N.Del_4$). From Figs. 11 and 12, we can see the good convergence between the *RBNN* expected data and FE data. The value of mean square error (MSE) between the *RBNN* expected data and FE data for scenarios ($N.Del_2$) and ($N.Del_4$), is 0.0695 and 0.0208

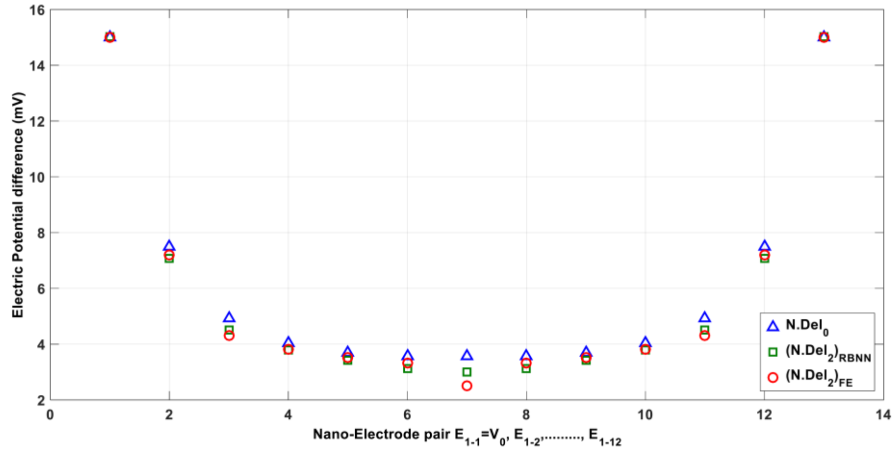

(a) Expected data

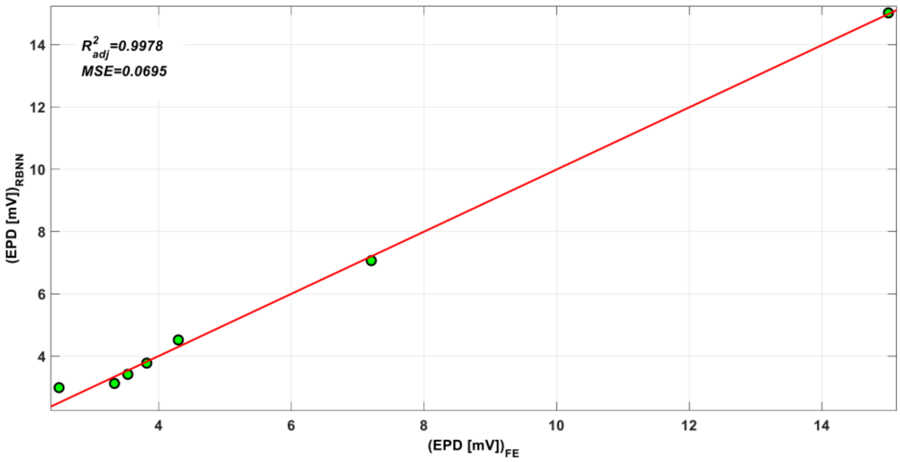

(b) Performance

Fig. 11 Comparison between the Finite Element (FE) data and Radial Basis neural networks (RBNN) expected data for nano-delamination scenario ($N.Del_2$)

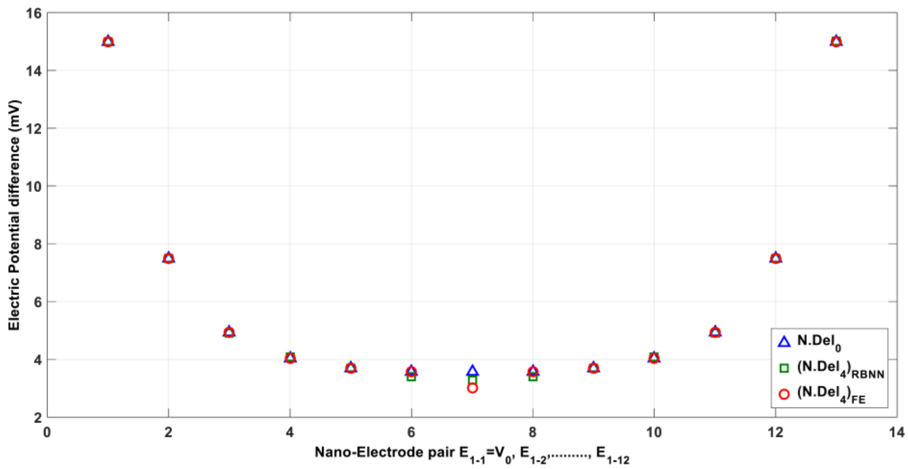

(a) Expected data

Fig. 12 Comparison between the Finite Element (FE) data and Radial Basis neural networks (RBNN) expected data for nano-delamination scenario ($N.Del_4$)

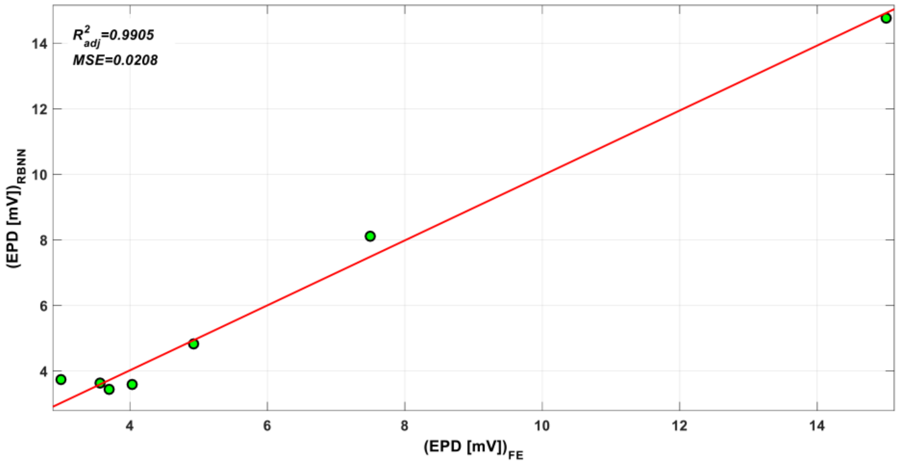

(b) Performance

Fig. 12 Continued

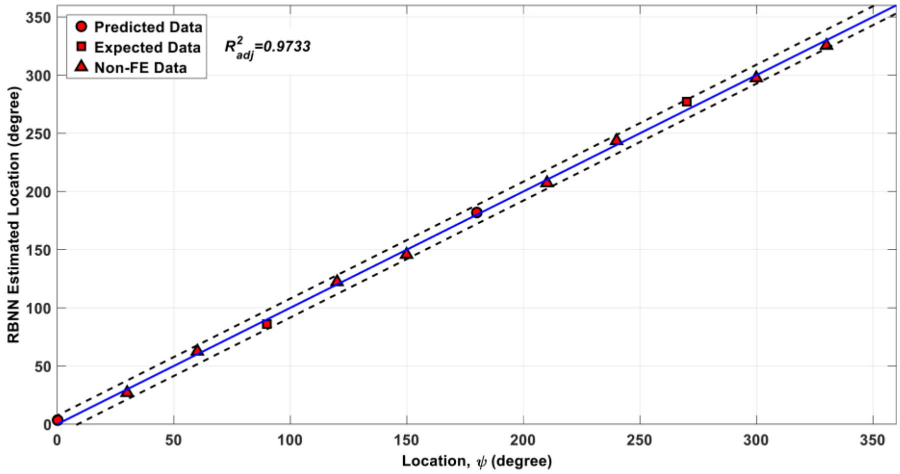

(a) Location, Ψ

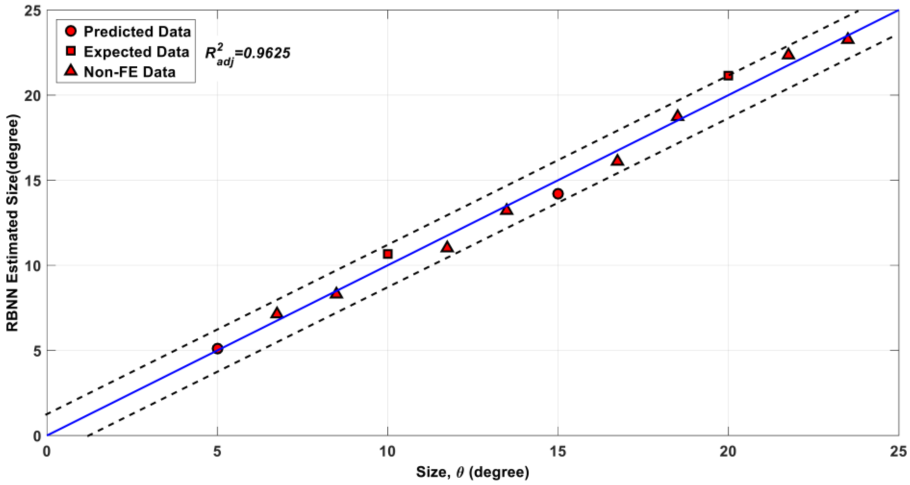

(b) Size, θ

Fig. 13 The Radial Basis neural networks (RBNN) Estimation results of nano-delamination (N.Del) in BFRP nano-pipe3 (*N.P*)

Table 5 Estimations and errors comparison between *RBNN* Data (unit degrees)

Nano-Delamination Scenario		RBNN Estimated Data		Error of Estimations	
				Size, θ	Location, Ψ
θ	Ψ	θ	Ψ	RBNN%	RBNN%
5	0	5.125[a]	3.332[a]	2.5[a]	3.332[a]
6.75	30	7.15[c]	27.24[c]	5.926[c]	9.2[c]
8.5	60	8.31[c]	62.8[c]	2.235[c]	4.667[c]
10	90	10.666[b]	86.153[b]	2.22[b]	4.274[b]
11.75	120	11.02[c]	122.34[c]	6.213[c]	1.95[c]
13.5	150	13.21[c]	145.47[c]	2.148[c]	3.02[c]
15	180	14.213[a]	182.112[a]	5.246[a]	1.173[a]
16.75	210	16.12[c]	207.11[c]	3.761[c]	1.3762[c]
18.5	240	18.72[c]	243.8[c]	1.189[c]	1.5833[c]
20	270	21.133[b]	276.938[b]	5.665[b]	2.5696[b]
21.75	300	22.34[c]	297.15[c]	2.713[c]	0.95[c]
23.5	330	23.24[c]	325.42[c]	1.106[c]	1.388[c]

[a] Predicted Data, [b] Expected Data, [c] Non-FE Data

respectively. The $R^2{}_{adj}$ of the expected result is 0.9978 and 0.9905 for scenarios (*N.Del*$_2$) and (*N.Del*$_4$) respectively.

5.5 The use of present RBNN for predicting non-FE data

The main target of artificial neural network design is the prediction of non-FE data. In this section, we will use the suggested *RBNN* to predict some non-EF data that is not included in the FE assessment. It is selected to use nine random *N.Del* location / size scenarios for all potential differences (EPD) E_{i-j}. The three previous parameters Ψ, θ, ε are the input vectors for the artificial neural network, while the output is the vector of the signal is the electric potential differences.

Fig. 13 shows the *RBNN* estimated results of the non-FE *N.Del* location, Ψ and size, *θ N.P*. The R^2_{adj} of non-FE result is 0.9733 and 0.9625 for location and size respectively. All of the estimations are plotted on the diagonal line.

The error band is defined as the maximum error of the estimated non-FE *N.Del* location/size. The error band from the diagonal line is less than 7.75 and 2.25 degrees for location and size respectively.

The estimated non-FE results of the location Ψ and size *θ* by *RBNN* are presented in Table 5. As a result, a *RBNN* gave good estimations for non-FE data even for extrapolations *N.Del* location/size in composite *N.P*.

6. Conclusions

In the present study, an electrical potential (EP) technique is adopted as an expert system for assessing *N.Del* location/size in *N.P* manufactured from Basalt Fiber Reinforced Polymer (BFRP) laminate composite using *ECS* with *ANNs*, which are combined to decrease detection effort to discern *N.Del* location/size inside the *N.P* layers, in order to keep the cost and save the time of the FE *N.Del* to keep the cost and save the time of the FE *N.Del* assessment data to a minimum with high accuracy, simple and low-cost. The results obtained are as follows:

(1) Electric potential difference due to different *N.Del* scenarios can be measured with multiple *N.Es* mounted on an outer surface of the *N.P*.
(2) The sensor sensitivity and assessment performance was found depend on the *N.Del* size (*θ*), as the *N.Del* size (*θ*) increases, the sensor sensitivity increased.
(3) The methodology has successfully monitored the *N.Del* location/size using only four scenarios of *N.Del* location/size are used for training the *ANNs* to estimate the non-FE results with good performance.
(4) The FE results are in excellent agreement with an *RBNN* results, thus validating the accuracy and reliability of the proposed technique, as shown in Table 5.
(5) *N.Del* size/ location assessment with *RBNN* can be successfully performed for non-FE *N.Del* size/ location scenarios in *N.P* with adjusted coefficient of multiple determination R^2_{adj} is 0. 0.9625 and 0.9733 respectively, see Fig. 13.
(6) The electrical potential (EP) technique with *ANNs* was gave good estimations of non-FE data even for extrapolations within the error band of less than 7.75 and 2.25 degree for *N.Del* location and size respectively, see Fig. 13.
(7) Finally, as a result, the proposed technique was successfully assessing the *N.Del* for a *N.P* with within low error band, and reduced the scenarios of *N.Del* to four scenarios only instead of 66 scenarios that must be used in other methods, This represents a significant saving of time and cost reduction associated with the electrical potential (EP) with *ANNs* method instead of the other methods.

References

Al-Tabey, W.A. (2010), "Effect of pipeline filling material on electrical capacitance tomography", *Proceedings of the International Postgraduate Conference on Engineering* (*IPCE 2010*), Perlis, Malaysia, October.

Al-Tabey, W.A. (2012), *Finite Element Analysis in Mechanical Design Using ANSYS*: *Finite Element Analysis* (*FEA*) *HandBook For Mechanical Engineers With ANSYS Tutorials*, LAP Lambert Academic Publishing, Germany (ISBN 978-3-8454-0479-0)

Al-tabey, W.A. (2014), "Vibration analysis of laminated composite variable thickness plate using finite strip transition matrix technique", In: *MATLAB Verifications MATLAB-Particular for Engineer* (Kelly, B., Ed.), InTech, USA, Volume 21, pp. 583-620. (ISBN 980–953-307-1128-8) https://doi.org/10.5772/57384

Altabey, W.A. (2016a), "Detecting and predicting the crude oil type inside composite pipes using ECS and ANN", *Struct*. *Monit*. *Maint*., *Int*. *J*., **3**(4), 377-393. http://dx.doi.org/10.12989/smm.2016.3.4.377

Altabey W.A. (2016b), "FE and ANN model of ECS to simulate the pipelines suffer from internal corrosion", *Struct*. *Monit*. *Maint*., **3**(3), 297-314. http://dx.doi.org/10.12989/smm.2016.3.3.297

Altabey, W.A. (2016c), "The thermal effect on electrical capacitance sensor for two-phase flow monitoring", *Struct*. *Monit*. *Maint*., *Int*. *J*., **3**(4), 335-347. http://dx.doi.org/10.12989/smm.2016.3.4.335

Altabey, W.A. (2017a), "An exact solution for mechanical behavior of BFRP Nano-thin films embedded in NEMS", J. *Adv*. *Nano Res*., *Int*. *J*., **5**(4), 337-357. https://doi.org/10.12989/anr.2017.5.4.337

Altabey, W.A. (2017b), "A study on thermo-mechanical behavior of MCD through bulge test analysis", *Adv*. *Computat*. *Des*., *Int*. *J*., **2**(2), 107-119. https://doi.org/10.12989/acd.2017.2.2.107

Altabey, W.A. (2017c), "Free vibration of basalt fiber reinforced polymer (FRP) laminated variable thickness plates with intermediate elastic support using finite strip transition matrix (FSTM) method", *J*. *Vibroeng*., **19**(4), 2873-2885. https://doi.org/10.21595/jve.2017.18154

Altabey, W.A. (2017d), "Prediction of natural frequency of basalt fiber reinforced polymer (FRP) laminated variable thickness plates with intermediate elastic support using artificial neural networks (ANNs) method", *J*. *Vibroeng*., **19**(5), 3668-3678. https://doi.org/10.21595/jve.2017.18209

Altabey, W.A. (2017e), "Delamination evaluation on basalt FRP composite pipe of electrical potential change", *Adv*. *Aircr*. *Spacecr*. *Sci*., *Int*. *J*., **4**(5), 515-528. http://dx.doi.org/10.12989/aas.2017.4.5.515

Altabey, W.A. (2017f), "EPC method for delamination assessment of basalt FRP pipe: Electrodes number effect", *Struct*. *Monit*. *Maint*., *Int*. *J*., **4**(1), 69-84. https://doi.org/10.12989/smm.2017.4.1.069

Altabey, W.A. (2018), "High performance estimations of natural frequency of basalt FRP laminated plates with intermediate elastic support using response surfaces method", *J*. *Vibroeng*., **20**(2), 1099-1107. https://doi.org/10.21595/jve.2017.18456

Altabey, W.A. and Noori, M. (2017), "Detection of fatigue crack in basalt FRP laminate composite pipe using electrical potential change method", *Proceedings of the 12th International Conference on Damage Assessment of Structures*, *IOP Conf*. *Series*: *Journal of Physics*, **842**, 012079, Kitakyushu, Japan, July.

Altabey, W.A. and Noori, M. (2018a), "Fatigue life prediction for carbon fibre/epoxy laminate composites under spectrum loading using two different neural network architectures", *Int*. *J*. *Sustain*. *Mater*. *Struct*. *Syst*., **3**(1), 53-78. http://dx.doi.org/10.1504/IJSMSS.2017.10013394

Altabey, W.A. and Noori, M. (2018b), "Monitoring the water absorption in GFRE pipes via an electrical capacitance sensors", *Adv*. *Aircr*. *Spacecr*. *Sci*., *Int*. *J*., **5**(4), 411-434. https://doi.org/10.12989/aas.2018.5.4.411

Altabey, W.A., Noori, M. and Wang, L. (2018a), *Using ANSYS for Finite Element Analysis*: *A Tutorial for Engineers*, Volume I, Momentum Press, USA (ISBN 978-1-94708-321-9).

Altabey, W.A., Noori, M. and Wang, L. (2018b), *Using ANSYS for Finite Element Analysis*: *Dynamic*, *Probabilistic*, *Design and Heat*, *Transfer Analysis*, Volume II, Momentum Press, USA (ISBN 978-1-94708-323-3)

Altabey, W.A., Noori, M., Zhao, Y. and Wu, Z. (2019), "Tensile creep monitoring of BFRP plates via electrical potential change and ANNs", *Sci*. *Iran*. *Trans B*: *Mech*. *Eng*. [In press].

ANSYS Low-Frequency Electromagnetic analysis Guide, The Electrostatic Module in the Electromagnetic subsection of ANSYS (2015), ANSYS, inc. Southpointe 275 Technology Drive Canonsburg, PA 15317, USA.

Asencio, K., Bramer-Escamilla, W., Gutiérrez, G. and Sánchez, I. (2015), "Electrical capacitance sensor array to measure density profiles of a vibrated granular bed", *J*. *Powder Technol*., **270**, 10-19. https://doi.org/10.1016/j.powtec.2014.10.003

Buhmann, M.D. (2003), *Radial Basis Functions*: *Theory and Implementations*, Cambridge University Press, Cambridge, UK.

Daoye, Y., Bin, Z., Chuanlong, X., Guanghua, T. and Shimin, W. (2009), "Effect of pipeline thickness on electrical capacitance tomography", *Proceedings of the 6th International Symposium on Measurement Techniques for Multiphase Flows*, *Journal of Physics*: *Conference Series*, **147**, 1-13, Okinawa, Japan, December.

Fasching, G.E. and Smith, N.S. (1988), "High resolution capacitance imaging system", US Dept. Energy, **37**, DOE/METC-88/4083.

Fasching, G.E. and Smith, N.S. (1991), "A capacitive system for 3-dimensional imaging of fluidized-beds", *Rev*. *Sci*. *Instr*., **62**(9), 2243-2251. https://doi.org/10.1063/1.1142343

Ghiasi, R., Ghasemi, M.R., Noori, M. and Altabey, W. (2019), "A non-parametric approach toward structural health monitoring for processing big data collected from the sensor network", *Structural Health Monitoring 2019*: *Enabling Intelligent Life-Cycle Health Management for Industry Internet of Things* (*IIOT*) - *Proceedings of the 12th International Workshop on Structural Health Monitoring* (*IWSHM 2019*), Stanford, CA, USA, September.

Huang, S.M., Plaskowski, A.B., Xie, C.G. and Beck, M.S. (1989), "Tomographic imaging of two-flow component flow using capacitance sensor", *J*. *Phys*. *E*: *Sci*. *Instrum*., **22**,173-177. https://doi.org/10.1088/0022-3735/22/3/009

Jaworski, A.J. and Bolton, G.T. (2000), "The design of an electrical capacitance tomography sensor for use with media of high dielectric permittivity", *Meas*. *Sci*. *Technol*., **11**(6), 743-757. https://doi.org/10.1088/0957-0233/11/6/318

Jiang, S., Li, D., Zhou, C. and Zhang, L. (2014), "Capabilities of stochastic response surface method and response surface method in reliability analysis", *Struct*. *Eng*. *Mech*., *Int*. *J*., **49**(1), 111-128. http://dx.doi.org/10.12989/sem.2014.49.1.111

Kost, A., Altabey W.A., Noori, M. and Awad, T. (2019), "Applying neural networks for tire pressure monitoring systems", *Struct*. *Durab*. *Health Monit*., **13**(3), 247-266. http://dx.doi.org/10.32604/sdhm.2019.07025

Li, H. and Huang, Z. (2000), *Special Measurement Technology and Application*, Zhejiang University Press, Hangzhou, China.

Mohamad, E.J., Rahim, R.A., Leow, P.L., Rahiman, M.H.F., Marwah, O.M.F., Nor Ayob, N.M., Rahim, H.A. and Mohd Yunus, F.R. (2012), "An introduction of two differential excitation potentials technique in electrical capacitance tomography", *Sensor*. *Actuat*. *A*, **180**, 1-10. https://doi.org/10.1016/j.sna.2012.03.025

Mohamad, E.J., Rahim, R.A., Rahiman, M.H.F., Ameran, H.L.M., Muji, S.Z.M. and Marwah, O.M.F. (2016), "Measurement and analysis of water/oil multiphase flow using electrical capacitance tomography sensor", *J. Flow Meas. Instrum.*, **47**, 62-70. https://doi.org/10.1016/j.flowmeasinst.2015.12.004

Mouritz, A.P. (2003), "Non-destructive evaluation of damage accumulation", Chapter 8 – *Fatigue in Composites*, (B. Harris), A volume in Woodhead Publishing Series in Composites Science and Engineering. (ISBN: 978-185573-608-5)

Myers, R. and Montgomery, D.C. (2002), *Response surface methodology process and product optimization using designed experiments*, (2nd Ed.), Wiley–Interscience, New York, USA

Noori, M., Wang, H., Altabey, W.A. and Silik, A.I.H. (2018), "A modified wavelet energy rate-based damage identification method for steel bridges", *Sci. Iran. Trans B: Mech. Eng.*, **25**(6), 3210-3230. https://doi.org/10.24200/sci.2018.20736

Pei, T. and Wang, W. (2009), "Simulation analysis of sensitivity for electrical capacitance tomography", *Proceedings of 9th International Conference on Electronic Measurement & Instruments* (*ICEMI 2009*), Beijing, China, August.

Sardeshpande, M.V., Harinarayan, S. and Ranade, V.V. (2015), "Void fraction measurement using electrical capacitance tomography and high speed photography", *J. Chem. Eng. Res. Des.*, **9**(4), 1-11. https://doi.org/10.1016/j.cherd.2014.11.013

Todoroki, A., Tanaka, Y. and Shimamura, Y. (2004), "Multi-prove electric potential change method for delamination monitoring of graphite/epoxy composite plates using normalized response surfaces", *Compos. Sci. Technol.*, **64**(5), 749-758. https://doi.org/10.1016/j.compscitech.2003.08.004

Valle, Y., Venayagamoorthy, G.K., Mohagheghi, S., Hernandez, J. and Harley, R.G. (2008). "Particle swarm optimization: basic concepts, variants and applications in power dystems", *IEEE Trans. Evol. Comput.*, **12**(2), 171-195. https://doi.org/10.1109/TEVC.2007.896686

Yang, W.Q., Stott, A.L., Beck, M.S. and Xie, C.G. (1995a), "Development of capacitance tomographic imaging systems for oil pipeline measurements", *Rev. Sci. Instrum.*, **66**(8), 4326. https://doi.org/10.1063/1.1145322

Yang, W.Q., Beck, M.S. and Byars, M. (1995b), "Electrical capacitance tomography–from design to applications", *Meas. Control*, **28**(9), 261-266. https://doi.org/10.1177/002029409502800901

Zhang, W., Wang, C., Yang, W. and Wang, C. (2014), "Application of electrical capacitance tomography in particulate process measurement – A review", *Adv. Powder Technol.*, **25**(1), 174-188. https://doi.org/10.1016/j.apt.2013.12.003

Zhao, Y., Noori, M. and Altabey, W.A. (2017a), "Damage detection for a beam under transient excitation via three different algorithms", *J. Struct. Eng. Mech.*, **64**(6), 803-817. https://doi.org/10.12989/sem.2017.64.6.803

Zhao, Y., Noori, M., Altabey, W.A. and Naiwei, L. (2017b), "Reliability evaluation of a laminate composite plate under distributed pressure using a hybrid response surface method", *Int. J. Reliabil. Quality Safe. Eng.*, **24**(3), 1750013. http://dx.doi.org/10.1142/S0218539317500139

Zhao, Y., Noori, M., Altabey W.A. and Wu, Z. (2018a), "Fatigue damage identification for composite pipeline systems using electrical capacitance sensors", *J. Smart Mater. Struct.*, **27**(8), 085023. https://doi.org/10.1088/1361-665X/aacc99

Zhao, Y., Noori, M., Altabey, W.A., Ghiasi, R. and Zhishen, W., (2018b), "Deep learning-based damage, load and support identification for a composite pipeline by extracting modal macro strains from dynamic excitations", *Appl. Sci.*, **8**(12), 2564. https://doi.org/10.3390/app8122564

Zhao, Y., Noori, M., Seyed, B.B. and Altabey, W.A. (2018c), "Mode shape-based damage identification for a reinforced concrete beam using wavelet coefficient differences and multi-resolution analysis", *J. Struct. Control Health Monit.*, **25**(1), e2041. https://doi.org/10.1002/stc.2041

Zhao, Y., Noori, M., Altabey, W.A., Ramin, G. and Wu, Z. (2019a), "Applying neural networks for tire pressure monitoring systems", *Struct. Durab. Health Monit.*, **13**(1), 85-103. http://dx.doi.org/10.32604/sdhm.2019.04695

Zhao, Y., Noori, M., Altabey, W.A. and Awad, T. (2019b), "A comparison of three different methods for the identification of hysterically degrading structures using BWBN model", *Front. Built Environ.*, **4**(80), 1-19. http://dx.doi.org/10.3389/fbuil.2018.00080

JL